

Effects of finite sizes of atomic nuclei on shear modulus and torsional oscillations in neutron stars

Hajime Sotani^{1,2} ^{*}, Hajime Togashi^{3,4} and Masatoshi Takano^{5,6}

¹*Astrophysical Big Bang Laboratory, RIKEN, Saitama 351-0198, Japan*

²*Interdisciplinary Theoretical & Mathematical Science Program (iTHEMS), RIKEN, Saitama 351-0198, Japan*

³*Department of Physics, Tohoku University, Sendai 980-8578, Japan*

⁴*Waseda Research Institute for Science and Engineering, Waseda University, Tokyo 169-8555, Japan*

⁵*Department of Physics, Waseda University, Tokyo 169-8555, Japan*

⁶*Institute for Advanced Theoretical and Experimental Physics, Waseda University, Tokyo 169-8555, Japan*

13 September 2022

ABSTRACT

The shear modulus of neutron star matter is one of the important properties for determining torsional oscillations in neutron stars. We take into account the effects of finite sizes of spherical nuclei on the shear modulus and examine the frequencies of crustal torsional oscillations. The shear modulus decreases owing to the finite-size effect, which in turn decreases the frequencies of torsional oscillations. In particular, the finite-size effect becomes more crucial for oscillations with a larger azimuthal quantum number and for neutron star models with a weaker density dependence of nuclear symmetry energy. In practice, when one identifies the quasi-periodic oscillations from a neutron star, where the magnetic effect is negligible, with crustal torsional oscillations, the finite-size effect can be more significant at frequencies higher than ~ 100 Hz.

Key words: asteroseismology – stars: neutron – stars: oscillations

1 INTRODUCTION

A neutron star produced through a supernova explosion is one of the most suitable environments for probing the physics under extreme states. The density inside neutron stars easily exceeds the standard nuclear density, and the gravitational and magnetic fields can be much stronger than those observed in our solar system (Shapiro & Teukolsky 1983). By observing neutron stars or their associated phenomena, one may obtain information that cannot be produced on Earth. For example, the discovery of $2M_{\odot}$ neutron stars excludes all the soft equations of state (EOSs), with which the expected maximum mass does not reach the observed masses (Demorest et al. 2010; Antoniadis et al. 2013; Cromartie et al. 2020). In addition, the pulsar light curve is affected by the general-relativistic light-bending effect, which primarily depends on stellar compactness, i.e., the ratio of the stellar mass to the stellar radius. Thus, by carefully observing the pulsar light curves, the mass and radius of neutron stars can be restricted (Riley et al. 2019, 2021; Miller et al. 2019, 2021). The resultant constraints are still largely uncertain, but they must be helpful in constraining the EOSs by accumulating the observational data on the mass and radius for additional objects. The gravitational wave event arising from the merging of binary neutron stars, GW170817 (Abbott et al. 2017a,b), also provides information on the constraint on tidal deformability, which indicates that the $1.4M_{\odot}$ neutron star radius should be less than 13.6 km (Annala et al. 2018).

The oscillation frequencies of neutron stars are another important piece of information. Since the oscillation spectrum strongly depends on the interior properties of an object, one may inversely obtain the interior information by observing the corresponding spectrum. This technique is known as asteroseismology. The asteroseismology of neutron stars was developed much earlier in order to interpret various possible neutron star oscillations detected in the electromagnetic spectrum (e.g., McDermott, Van Horn, & Hansen (1988)). Even now, the most important results of asteroseismology are those associated with electromagnetic observations, e.g., quasi-periodic oscillations (QPOs) from soft-gamma repeaters (SGRs) as we will describe

* E-mail: sotani@yukawa.kyoto-u.ac.jp

below. Furthermore, it has been proposed that the neutron star mass, radius, and EOS can be constrained by observing the gravitational waves from isolated compact objects (e.g., Andersson & Kokkotas (1996, 1998); Sotani, Tominaga & Maeda (2001); Sotani, Kohri & Harada (2004); Sotani et al. (2011); Doneva et al. (2013); Sotani (2021); Sotani & Kumar (2021); Sotani & Dohi (2022)). Regarding the gravitational asteroseismology of neutron stars, the important role of r -modes in rapidly rotating neutron stars has also been often discussed (e.g., Andersson & Kokkotas (2001)). Additionally, to understand the gravitational wave signals appearing in the numerical simulation of a core-collapse supernova explosion, asteroseismology has recently been adopted (e.g., Morozova et al. (2018); Sotani et al. (2019); Sotani & Sumiyoshi (2019); Torres-Forné et al. (2019); Sotani, Takiwaki & Togashi (2021)). Gravitational waves from isolated neutron stars have never been detected yet, but once they can be directly observed, one may be able to extract neutron star properties by asteroseismology. Instead of gravitational waves, however, several QPO frequencies have been detected in the x-ray afterglow following giant flares from SGRs, e.g., SGR 1900+14 and SGR 1806-20, whose frequencies are in the range of a few tenths of Hz up to kHz (Strohmayer & Watts 2005, 2006). If one assumes that these QPOs come from crustal torsional oscillations in a neutron star, one can constrain the crust properties (e.g., Steiner & Watts (2009); Gearheart et al. (2011); Passamonti & Andersson (2012); Sotani et al. (2012, 2013a,b); Sotani (2014); Sotani, Iida & Oyamatsu (2016, 2017a, 2018, 2019)), even though the emission mechanism of QPOs is not understood yet. We note that, since the SGRs are magnetars, i.e., highly magnetized neutron stars, one may have to take into account the magnetic field effect on torsional oscillations. In fact, the frequencies of crustal torsional oscillations increase as the field strength increases (Sotani, Kokkotas & Stergioulas 2007; Gabler et al. 2013). Then, eventually, the crustal torsional oscillations disappear and Alfvén oscillations become dominant as the magnetar oscillations. Nevertheless, considering the observational estimation of the magnetic field strength of SGR 1900+14 and SGR 1806-20 inferred from the spin-down rate (Kouveliotou et al. 1998; Hurley et al. 1999), the crustal torsional oscillations must still survive.

Crustal torsional oscillations are characterized by the shear modulus in the crust region. The shear modulus is a property associated with rigidity against distortion. Therefore, it is mainly determined by the lattice energy in the crust. In the phase composed of spherical nuclei in the crust, where the nuclei form a body-centered cubic (bcc) lattice, the shear modulus for zero-temperature matter has been formulated as a function of the ion number density and charge of a nucleus (Strohmayer et al. 1991) (see section 2 for details). However, in deriving the formula of the shear modulus, it is assumed that the nuclei in the crust are point-like particles. Indeed, this assumption may be valid for the nuclei in the outer crust, where neutrons are still confined in the nuclei, whereas the finite-size effect of nuclei must become non-negligible in the inner crust. Thus, in this paper, we first consider the shear modulus in the bcc lattice by including the finite-size effect of the nuclei and then discuss this effect on the frequency of crustal torsional oscillations in a nonmagnetized neutron star. The so-called pasta phase composed of nonspherical nuclei also contributes to crustal torsional oscillations (e.g., Sotani, Iida & Oyamatsu (2018, 2019)), but the thickness of such a phase is much smaller than that of the phase composed of spherical nuclei. Therefore, in this paper, we simply consider crustal torsional oscillations, whose restoring force comes from only the elasticity of the lattice structure with spherical nuclei. We note that the torsional oscillations are confined inside the crust region because the shear modulus vanishes inside the core region, where the matter behaves as a fluid.

2 SHEAR MODULUS

The elasticity of the neutron star crust is characterized by the shear modulus. The shear modulus in the bcc lattice composed of spherical nuclei, which are the main components of the crust region, is approximately described in the limit of zero temperature as

$$\mu_0 = 0.1194 \frac{n_i(Ze)^2}{a}, \quad (1)$$

where n_i , Z , and a denote the ion number density, charge number of the ion, and the radius of a Wigner–Seitz cell, respectively, i.e., $4\pi a^3/3 = 1/n_i$ (Strohmayer et al. 1991). We note that this expression has been derived by averaging the overall direction of infinitesimal displacements with respect to the shear motion under the assumption that each spherical nucleus is only a point charge (Ogata & Ichimaru 1990). In Eq. (1), one can observe that the shear modulus in the bcc lattice is proportional to the lattice (or Coulomb) energy. In fact, the shear modulus in two-dimensional geometry is directly expressed by the Coulomb energy in equilibrium (Pethick & Potekhin 1998).

To take into account the size effect of spherical nuclei on the shear modulus, we assume the situation that the protons distribute uniformly with the density n_p in the region of $r \leq r_p$, where r_p is the reference proton radius defined by $4\pi r_p^3 n_p/3 = Z$. We note that the neutron radius r_n is generally not equivalent to r_p , and the difference $r_n - r_p$ is the neutron skin thickness. Then, the lattice energy W_L of the unit cell within the Wigner–Seitz approximation for the compressible liquid drop model is written as (Baym, Bethe & Pethick 1971)

$$W_L = -\frac{9Z^2 e^2}{10a} f_L, \quad (2)$$

where f_L is a function of r_p/a given as

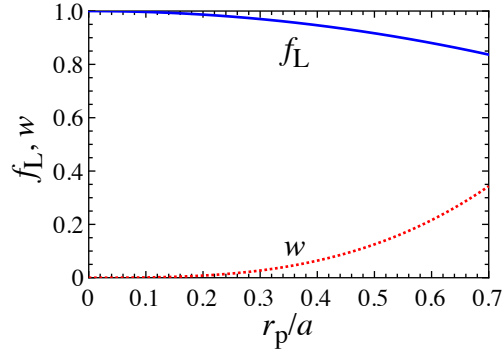


Figure 1. The contribution function of the finite-size effect of spherical nuclei (f_L) and the volume fraction (w) are plotted as functions of the ratio of the reference proton radius to the radius of a Wigner–Seitz cell, where the solid and dotted lines correspond to f_L and w , respectively.

$$f_L = 1 - \frac{1}{3} \left(\frac{r_p}{a} \right)^2. \quad (3)$$

Here, W_L in the limit of $r_p = 0$, where $f_L = 1$, becomes the lattice energy with point-like nuclei, i.e., f_L corresponds to a contribution function of the finite-size effect of spherical nuclei. In Fig. 1, we show the behavior of f_L and the volume fraction $w \equiv (r_p/a)^3$ as a function of r_p/a . From this figure, one can observe that the lattice energy slightly depends on the size of spherical nuclei. Since the ratio of r_p to a (or the volume fraction) generally increases with density, one can observe the stronger finite-size effect of the nuclei in the higher-density region. Since the shear modulus is directly associated with lattice energy as mentioned above, it would be natural to express the shear modulus including the finite-size effect of spherical nuclei, μ_f , as

$$\mu_f = \mu_0 f_L. \quad (4)$$

Furthermore, nuclei may deform during the shear motion. If so, one has to take into account the effect of nuclear deformation on the shear modulus in the case of the finite-size nuclei. In fact, since the timescale of strong interactions (associated with the deformation) is much smaller than that of the Coulomb interaction, nuclei can deform, depending on their position. However, it is unclear how large the deformation of nuclei is during the shear motion because the amplitude of shear oscillations is not constrained by the observations. Thus, in this study, we simply adopt Eq. (4) as the shear modulus in the case of finite-size nuclei. We note that the phonon contribution to the shear modulus (Baiko 2011), the electron screening effect on the shear modulus (Kobyakov & Pethick 2013), and the elastic properties of polycrystals (Kobyakov & Pethick 2015) have been studied as other effects, but we simply neglect such effects in this study. We also note that the total Coulomb energy of a unit cell within the Wigner–Seitz approximation for a compressible liquid drop model is written as

$$E_{\text{Coul}} = \frac{3Z^2 e^2}{5r_p} + W_L = \frac{3Z^2 e^2}{5r_p} f_C, \quad (5)$$

where f_C is a contribution function of the finite-size effect of spherical nuclei given as

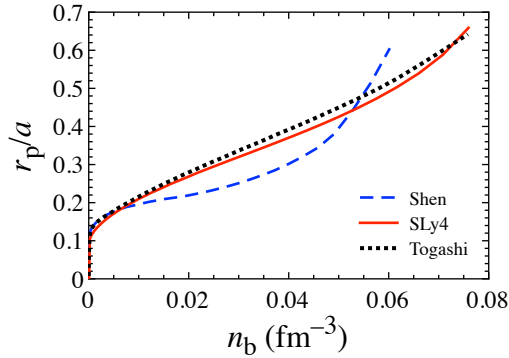
$$f_C = 1 - \frac{3}{2} \frac{r_p}{a} + \frac{1}{2} \left(\frac{r_p}{a} \right)^3. \quad (6)$$

One may think that the shear modulus including the finite-size effect is constructed with f_C instead of f_L shown in Eq. (4), where the dependence of f_C on r_p/a is stronger than that of f_L . In this study, however, we employ f_L as shown in Eq. (4).

To examine how the frequencies of torsional oscillations depend on the EOSs, in this study, we adopt three different EOSs listed in Table 1, i.e., the EOS based on the relativistic mean-field (Shen EOS) (Shen et al. 1998, 2011), the EOS with the Skyrme-type interaction (SLy4 EOS) (Douchin & Haensel 2001), and the EOS derived by the variational method (Togashi EOS) (Togashi et al. 2017). The derivation of the reference proton radius r_p used in Eq. (3) for the SLy4 EOS is different from that for the other EOSs. That is, the SLy4 EOS was constructed within the compressible liquid drop model for non-uniform matter in the neutron star crust, so r_p can be strictly defined in the model. On the other hand, the Thomas–Fermi approximation was adopted to construct the Shen and Togashi EOSs for non-uniform matter, where the diffuseness of the nuclear surface was taken into account. For the Shen and Togashi EOSs, therefore, r_p used in this study is evaluated so that the root-mean-square proton radius calculated in the Thomas–Fermi approximation reproduces that in the compressible liquid drop model with r_p . In Fig. 2, the ratio of r_p to a for different EOSs is shown as a function of the baryon number density, where the dashed, solid, and dotted lines denote the results obtained using the Shen, SLy4, and Togashi EOSs, respectively. The values of r_p obtained using the Shen and Togashi EOSs are reasonable as compared with that obtained using the SLy4 EOS.

Table 1. EOS parameters adopted in this study, the maximum gravitational mass M_{max} for a cold neutron star constructed with the corresponding EOSs, and the density at the bottom edge of the neutron star crust, n_{sp} .

EOS	K_0 (MeV)	L (MeV)	η (MeV)	M_{max}/M_{\odot}	n_{sp} (fm^{-3})
Shen	281	111	151	2.17	0.0602
SLy4	230	45.9	78.5	2.05	0.0760
Togashi	245	38.7	71.6	2.21	0.0758

**Figure 2.** The ratio r_p/a is shown as a function of the baryon number density for different EOSs, where the dashed, solid, and dotted lines correspond to the results obtained using the Shen, SLy4, and Togashi EOSs, respectively.

We note that the constraint on the $1.4M_{\odot}$ neutron star radius obtained from GW170817 has excluded the Shen EOS (Annala et al. 2018), but we still consider this EOS to examine the EOS dependence of the frequencies of torsional oscillations. In Table 1, we list the EOS parameters, where K_0 is the incompressibility of the symmetric nuclear matter, L is the density dependence of nuclear symmetry energy, and η is given by $\eta \equiv (K_0 L^2)^{1/3}$ (a suitable combination for expressing low-mass neutron stars proposed by Sotani et al. (2014)). In addition, we also list the maximum mass and the transition density from the phase composed of spherical nuclei to uniform matter, i.e., the density at the bottom of the inner crust. We note that fission-like instability occurs when the volume fraction w reaches $\sim 1/8$ (Pethick & Ravenhall 1995), which leads to the phase transition from the spherical nuclei phase to the so-called pasta phase and eventually to uniform matter, as the density increases. Even so, since the thickness of the pasta phase is much smaller than that of the phase composed of spherical nuclei (Sotani, Iida & Oyamatsu 2017b), we simply neglect the existence of the pasta phase in this study. This assumption is expected to be valid at least for the EOSs adopted in this study for the following reasons: The crustal torsional oscillations are confined inside the phase of spherical and cylindrical nuclei, since the slab-like nuclei behave as fluid against linear perturbation (Pethick & Potekhin 1998). Furthermore, the frequencies inside the phase of spherical nuclei are almost the same as those in the phase of spherical and cylindrical nuclei when one considers the EOS with $L \gtrsim 40$ MeV, which was confirmed by Sotani, Iida & Oyamatsu (2018).

In Fig. 2, the ratio of r_p to a increases with density, which becomes more than $\sim 60\%$ at the bottom of the crust independently of the EOS. One also observes the EOS dependence (or L -dependence) in the profile of r_p/a , i.e., r_p/a for an EOS with larger L tends to be smaller. This is because the symmetry energy at subnuclear density becomes smaller for an EOS with a larger L , which decreases the charge number of nuclei. The top panel in Fig. 3 shows the shear modulus with and without the finite-size effect for the neutron star model constructed with the Togashi EOS; μ_f becomes smaller than μ_0 as the density increases owing to the finite-size effect. The bottom panel in Fig. 3 shows the relative deviations of the shear modulus for different EOSs; the deviations amount to $\sim 15\%$ at around the bottom of the crust. We also note that the EOS dependence of the relative deviation shown in the bottom panel in Fig. 3 is very similar to that of r_p/a , as expected.

3 TORSIONAL OSCILLATIONS

In this study, we simply consider a neutron star without a magnetic field. As mentioned above, since the torsional oscillations excited in a nonmagnetized neutron star are confined inside the neutron star crust, we focus only on the crust region. Spherically symmetric neutron star models are generally constructed by integrating the Tolman–Oppenheimer–Volkoff (TOV) equations together with an appropriate EOS from the center up to the surface outward, for a given central density. On the other hand,

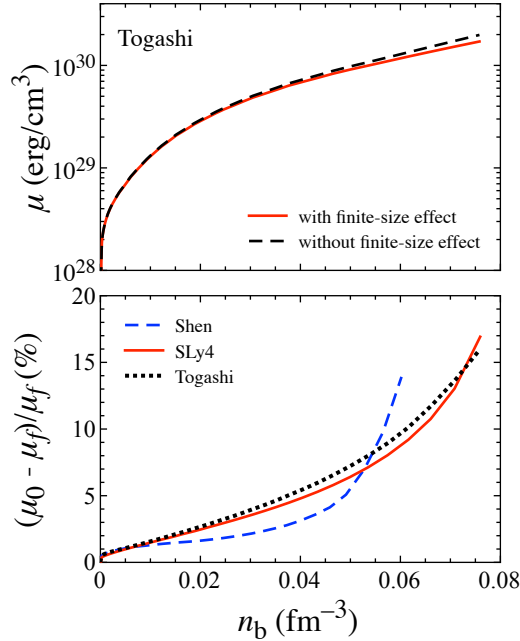


Figure 3. Shear moduli with and without the finite-size effect are respectively shown with the solid and dashed lines as a function of the baryon number density for the Togashi EOS in the top panel. In the bottom panel, we show the relative deviation of the shear modulus without the finite-size effect (μ_0) to that with the finite-size effect (μ_f) for different EOSs, where the dashed, solid, and dotted lines correspond to the results obtained using the Shen, SLy4, and Togashi EOSs, respectively.

to eliminate uncertainties in the EOS for the higher-density region, which corresponds to the neutron star core region, in this study, we construct the neutron star crust by integrating the TOV equations inward from the stellar surface down to the bottom edge of the crust for selected values of stellar mass and radius, as in Sotani et al. (2012, 2013a). In such a crust model, we consider the torsional oscillations.

Since the crustal torsional oscillations are of the axial type, the relativistic Cowling approximation works well, i.e., the metric perturbations during the oscillations can be omitted. The perturbation equation for the angular displacement can be derived from the linearized equation of motion (Schumaker & Thorne 1983). Since the core region of a neutron star behaves as a fluid, torsional oscillations are confined only to the crust region. Thus, the boundary conditions are imposed on the bottom edge of the crust and at the stellar surface. In practice, we adopt the zero-traction condition at the bottom edge of the crust and the zero-torque condition at the stellar surface (Schumaker & Thorne 1983; Sotani, Kokkotas & Stergioulas 2007). The concrete perturbation equation and boundary conditions are shown in Sotani et al. (2012). Then, the problem to solve becomes an eigenvalue problem.

As shown in Fig. 3, the shear modulus decreases owing to the finite-size effect. As a result, since the shear velocity given by $(\mu/(\varepsilon + p))^{1/2}$ with the energy density ε and pressure p also decreases, one can expect that the frequencies of torsional oscillations with the finite-size effect become smaller than those without the effect. In Fig. 4, we show the relative deviation Δ given as

$$\Delta = \frac{\ell f_n^{(-)} - \ell f_n^{(+)}}{\ell f_n^{(+)}} \quad (7)$$

where $\ell f_n^{(+)}$ and $\ell f_n^{(-)}$ respectively correspond to the frequencies of the ℓ -th torsional oscillations with and without the finite-size effect, while n denotes the nodal number in the eigenfunction. Since the results obtained using the SLy4 EOS are almost the same as those obtained using the Togashi EOS, hereafter we focus only on the results obtained using the Shen and Togashi EOSs. From this figure, one can observe that the frequencies decrease owing to the finite-size effect, as expected, but the relative deviation Δ is almost independent of ℓ . One also finds that the relative deviation in the fundamental frequencies ($n = 0$) decreases for the neutron star model with a larger L , which is caused by the L -dependence in the shear modulus as shown in Fig. 3, whereas the relative deviation in overtones does not seem to be very simple because the frequencies of overtones depend on not only the shear modulus but also the crust thickness (Hansen & Cioffi 1980)¹. However, the fundamental oscillations

¹ We also note that, for strongly magnetized neutron stars, the frequency modulation due to the fine-size effect of atomic nuclei as shown in Fig. 4 is much smaller than that due to the magnetic fields (e.g., Sotani, Kokkotas & Stergioulas (2007); Gabler et al. (2013)).

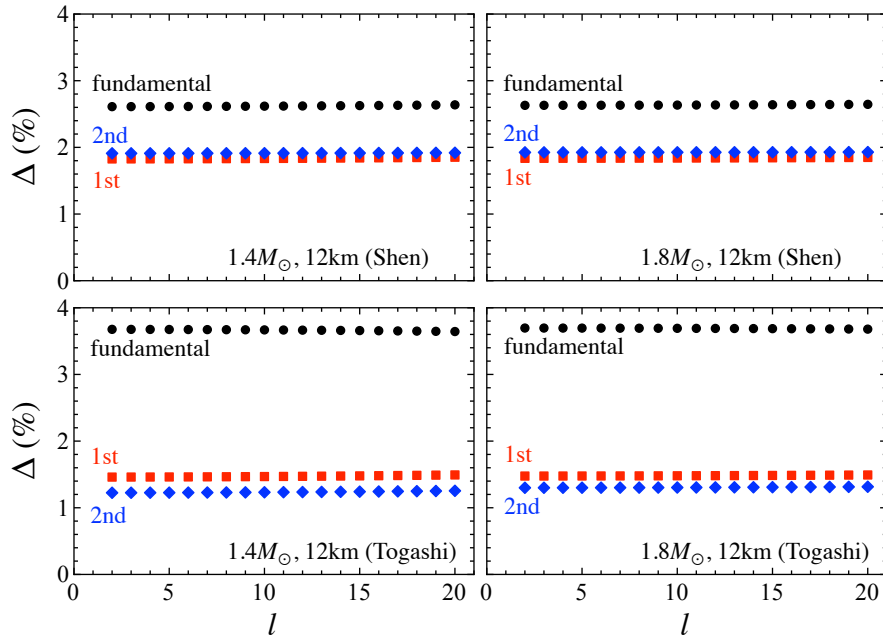


Figure 4. The relative deviation of frequencies without the finite-size effect from those with such an effect, defined by Eq. (7), is shown as a function of ℓ , where the circles, squares, and diamonds denote the results for the fundamental oscillations ($n = 0$) and the 1st ($n = 1$) and 2nd overtones ($n = 2$), respectively. The left and right panels correspond to the neutron star model with $1.4M_{\odot}$ and $1.8M_{\odot}$, whereas the top and bottom panels correspond to the neutron star model constructed from the results obtained using the Shen and Togashi EOSs, respectively.

may be more important, if one is going to identify the QPO frequencies from a neutron star with crustal torsional oscillations. In fact, the frequencies observed in magnetar giant flares, such as SGR 1806-20 or SGR 1900+14, range from ~ 10 Hz up to the order of kilohertz, among which the frequencies of about 100 Hz, e.g., 150 Hz in SGR 1806-20 or 155 Hz in SGR 1900+14, are the most suitable ones to be identified with the fundamental frequencies of the crustal torsional oscillations for certain values of ℓ (see Sotani et al. (2012, 2013a)). In the following, therefore, we focus on fundamental oscillations.

Although the relative deviation Δ is almost independent of ℓ as shown in Fig. 4, the absolute value of the deviation of frequency increases with ℓ because the fundamental frequency itself increases with ℓ . To choose the value of ℓ above which the finite-size effect is not negligible, we examine the following two quantities, i.e., δf_1 , which is the deviation between the ℓ -th and $(\ell - 1)$ -th fundamental frequencies without the finite-size effect, and δf_2 , which is the deviation between the ℓ -th fundamental frequencies without and with the finite-size effect. Explicitly, they are given by

$$\delta f_1(\ell) = {}_{\ell}f_0^{(-)} - {}_{\ell-1}f_0^{(-)}, \quad (8)$$

$$\delta f_2(\ell) = {}_{\ell}f_0^{(-)} - {}_{\ell}f_0^{(+)}. \quad (9)$$

The resultant values of δf_1 and δf_2 are shown in Fig. 5, where the filled and open circles respectively correspond to δf_1 and δf_2 . As seen in this figure, δf_2 increases with ℓ , which means that the finite-size effect becomes more important as ℓ increases. In fact, we show the ℓ value above which $\delta f_2/\delta f_1$ becomes larger than 0.5 with the vertical dashed line in Fig. 5 for reference. For the neutron star model constructed using the Togashi, SLy4, and Shen EOSs, the corresponding ℓ values are 12, 13, and 19, respectively. This implies that the finite-size effect becomes more important for the stellar model with a smaller L .

4 CONCLUSION

The QPOs observed in the afterglow following magnetar giant flares are considered to be strongly associated with neutron star oscillations. One of the possible theoretical explanations of the observations is crustal torsional oscillations, in which the oscillation frequencies are governed by the shear modulus. The shear modulus in the bcc lattice composed of spherical nuclei is well known and formulated under the assumption that the nuclei are point-like particles. In this study, we focus on the finite-size effect of spherical nuclei and take it into account the value of the shear modulus. The shear modulus decreases owing to the finite-size effect, which is more important for EOSs with a smaller L . We also examine the frequencies of crustal torsional oscillations in a nonmagnetized neutron star to evaluate the finite-size effect. We find that the finite-size effect becomes more crucial in torsional oscillations with a larger ℓ and in the neutron star models constructed using the EOSs

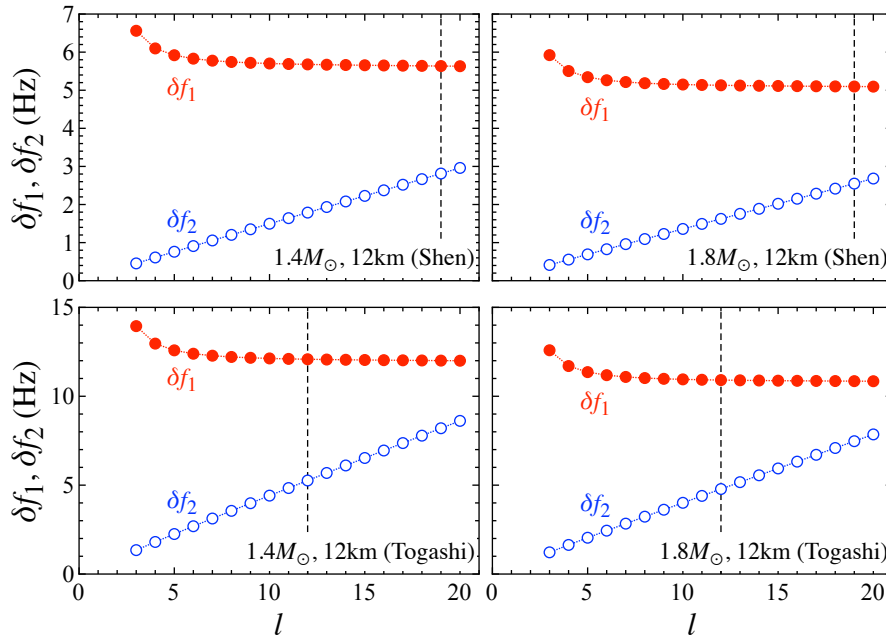


Figure 5. The deviations of the frequencies, δf_1 and δf_2 , are shown as a function of ℓ , where δf_1 and δf_2 are given by Eqs. (8) and (9), respectively. The vertical dashed line denotes the values of ℓ at which the ratio of δf_2 to δf_1 , i.e., $\delta f_2/\delta f_1$, becomes more than 0.5.

with a smaller L . In practice, if one identifies the observed QPO frequencies with crustal torsional oscillations, the finite-size effect is not negligible for QPOs of more than ~ 100 Hz. We note that the QPO frequencies detected in the afterglow of magnetar giant flares can be more strongly affected by magnetic fields (e.g., Sotani, Kokkotas & Stergioulas (2007); Gabler et al. (2013)) than by the finite-size effects. Therefore, the latter effects would be more pronounced if QPOs associated with torsional oscillations were detected from weakly magnetized neutron stars.

ACKNOWLEDGEMENTS

We would like to express our special thanks to H. Shen for providing us with numerical data on parameters of the Thomas-Fermi calculation. This work was supported in part by Japan Society for the Promotion of Science (JSPS) KAKENHI Grant Numbers JP18K13551, JP19KK0354, JP20H04753, JP21H01088, and JP21K13924 and by Pioneering Program of RIKEN for Evolution of Matter in the Universe (r-EMU).

DATA AVAILABILITY

The data underlying this article will be shared on reasonable request to the corresponding author.

REFERENCES

- Abbott B. P. et al. (LIGO Scientific Collaboration and Virgo Collaboration), 2017a, Phys. Rev. Lett., 119, 161101
- Abbott B. P. et al. (LIGO Scientific Collaboration and Virgo Collaboration), 2017b, ApJ, 848, L12
- Andersson N., Kokkotas K. D., 1996, Phys. Rev. Lett., 677, 4134
- Andersson N., Kokkotas K. D., 1998, MNRAS, 299, 1059
- Andersson N., Kokkotas K. D., 2001, Int. J. Mod. Phys. D, 10, 381
- Annala E., Gorda T., Kurkela A., Vuorinen A., 2018, Phys. Rev. Lett., 120, 172703
- Antoniadis J. et al., 2013, Science, 340, 6131
- Baiko D. A., 2011, MNRAS, 416, 22
- Baym G., Bethe H. A., Pethick C. J., 1971, Nucl. Phys. A, 175, 225
- Cromartie H. T. et al., 2020, Nat. Astron., 4, 72
- Demorest P., Pennucci T., Ransom S., Roberts M., Hessels J., 2010, Nature, 467, 1081
- Doneva D. D., Gaertig E., Kokkotas K. D., Krüger C., 2013, Phys. Rev. D, 88, 044052

- Douchin F., Haensel P., 2001, *A&A*, 380, 151
- Gabler M., Cerdá-Durán P., Font J. A., Müller E., Stergioulas N., 2013, *MNRAS*, 430, 1811
- Gearheart M., Newton W. G., Hooker J., Li B. A., 2011, *MNRAS*, 418, 2343
- Hansen C., Cioffi D. F., 1980, *ApJ*, 238, 740
- Hurley K. et al., 1999, *ApJ*, 510, L111
- Kobyakov D., Pethick C. J., 2013, *Phys. Rev. C*, 87, 055803
- Kobyakov D., Pethick C. J., 2015, *MNRAS*, 449, L110
- Kouveliotou C. et al., 1998, *Nature*, 393, 235
- McDermott P. N., Van Horn H. M., Hansen C. J., 1988, *ApJ*, 325, 725
- Miller M. C. et al., 2019, *ApJ*, 887, L24
- Miller M. C. et al., 2021, *ApJ*, 918, L28
- Morozova V., Radice D., Burrows A., Vartanyan D., 2018, *ApJ*, 861, 10
- Ogata S., Ichimaru S., 1990, *Phys. Rev. A*, 42, 4867
- Passamonti A., Andersson N., 2012, *MNRAS*, 419, 638
- Pethick C. J., Potekhin A. Y., 1998, *Phys. Lett. B*, 427, 7
- Pethick C. J., Ravenhall D. G., 1995, *Annu. Rev. Nucl. Part. Sci.*, 45, 429
- Riley T. E. et al., 2019, *ApJ*, 887, L21
- Riley T. E. et al., 2021, *ApJ*, 918, L27
- Schumaker B. L., Thorne K. S., 1983, *MNRAS*, 203, 457
- Shapiro S. L., Teukolsky S. A., in *Black Holes, White Dwarfs, and Neutron Stars* (A Wiley-Interscience Publication, 1983)
- Shen H., Toki H., Oyamatsu K., Sumiyoshi K., 1998, *Nucl. Phys. A*, 637, 435
- Shen H., Toki H., Oyamatsu K., Sumiyoshi K., 2011, *ApJS*, 197, 20
- Sotani H., 2014, *Phys. Lett. B*, 730, 166
- Sotani H., 2021, *Phys. Rev. D*, 103, 123015
- Sotani H., Kumar B., 2021, *Phys. Rev. D*, 104, 123002
- Sotani H., Dohi A., 2022, *Phys. Rev. D*, 105, 023007
- Sotani H., Iida K., Oyamatsu K., 2016, *New Astron.*, 43, 80
- Sotani H., Iida K., Oyamatsu K., 2017a, *MNRAS*, 464, 3101
- Sotani H., Iida K., Oyamatsu K., 2017b, *MNRAS*, 470, 4397
- Sotani H., Iida K., Oyamatsu K., 2018, *MNRAS*, 479, 4735
- Sotani H., Iida K., Oyamatsu K., 2019, *MNRAS*, 489, 3022
- Sotani H., Iida K., Oyamatsu K., Ohnishi A., 2014, *Prog. Theor. Exp. Phys.* 2014, 051E01
- Sotani H., Kohri K., Harada T., 2004, *Phys. Rev. D*, 69, 084008
- Sotani H., Kokkotas K. D., Stergioulas N., 2007, *MNRAS*, 375, 261
- Sotani H., Kuroda T., Takiwaki T., Kotake K., 2019, *Phys. Rev. D*, 99, 123024
- Sotani H., Nakazato K., Iida K., Oyamatsu K., 2012, *Phys. Rev. Lett.*, 108, 201101
- Sotani H., Nakazato K., Iida K., Oyamatsu K., 2013a, *MNRAS*, 428, L21
- Sotani H., Nakazato K., Iida K., Oyamatsu K., 2013b, *MNRAS*, 434, 2060
- Sotani H., Sumiyoshi K., 2019, *Phys. Rev. D*, 100, 083008
- Sotani H., Takiwaki T., Togashi H., 2021, *Phys. Rev. D*, 104, 123009
- Sotani H., Tominaga K., Maeda K. I., 2001, *Phys. Rev. D*, 65, 024010
- Sotani H., Yasutake N., Maruyama T., Tatsumi T., 2011, *Phys. Rev. D*, 83, 024014
- Steiner A. W., Watts A. L., 2009, *Phys. Rev. Lett.*, 103, 181101
- Strohmayer T., van Horn H. M., Ogata S., Iyetomi H., Ichimaru S., 1991, *ApJ*, 375, 679
- Strohmayer T. E., Watts A. L., 2005, *ApJ*, 632, L111
- Strohmayer T. E., Watts A. L., 2006, *ApJ*, 653, 593
- Togashi H., Nakazato K., Takehara Y., Yamamuro S., Suzuki H., Takano M., 2017, *Nucl. Phys. A*, 961, 78
- Torres-Forné A., Cerdá-Durán P., Passamonti A., Obergaulinger M., Font J. A., 2019, *MNRAS*, 482, 3967